Supporting Information for

Direct oxygen atom transfer *versus* electron transfer mechanisms in the phosphine oxidation by nonheme Mn(IV)-oxo complexes

Yong-Min Lee,[a‡] Mi Yoo,[a‡] Heejung Yoon,[b] Xiao-Xi Li,[a]

Wonwoo Nam*[a] and Shunichi Fukuzumi*[abc]

[a] *Department of Chemistry and Nano Science, Ewha Womans University, Seoul 03760, Korea.*

E-mail: fukuzumi@chem.eng.osaka-u.jp, wwnam@ewha.ac.kr

[b] *Department of Material and Life Science, Graduate School of Engineering, Osaka University, Suita, Osaka 565-0871, Japan*

[c] *Faculty of Science and Technology, Meijo University, SENTAN, Japan Science and Technology Agency (JST), Nagoya, Aichi 468-8502, Japan*

‡ *These authors contributed equally to this work.*

E-mail: wwnam@ewha.ac.kr, fukuzumi@chem.eng.osaka-u.ac.jp

Experimental Section

Materials. Commercially available chemicals were used without further purification unless otherwise indicated. Solvents were dried according to published procedures and distilled under Ar prior to use.[S1] Iodosylbenzene (PhIO) was prepared by a literature method.[S2] Bn-TPEN ligand (Bn-TPEN = *N*-benzyl-*N*,*N*',*N*'-tris(2-pyridylmethyl)-1,2-diaminoethane) and $Mn^{II}(CF_3SO_3)_2 \cdot 2CH_3CN$ were prepared by literature methods.[S3] Mn^{II}(Bn-TPEN)$(CF_3SO_3)_2$ was synthesized in a glove box according to the literature;[S4] Bn-TPEN ligand (0.47 mmol, 200 mg) and $Mn^{II}(CF_3SO_3)_2 \cdot 2CH_3CN$ (0.57 mmol, 250 mg) were dissolved in CH_3CN and stirred at ambient temperature overnight. The resulting solution was filtered and added to a large volume of Et_2O. The product was obtained as a white solid with 83% yield (0.37 g). $[(\text{Bn-TPEN})Mn^{IV}(O)]^{2+}$ (**1**) was generated by reacting Mn^{II}(Bn-TPEN)$(CF_3SO_3)_2$ and PhIO (4 equiv.) in CF_3CH_2OH/MeCN (1:1 v/v) at 273 K and then complex **2** was generated by adding HOTf (30 mM) to a solution of **1**, as reported previously.[S4]

Instrumentation. UV-vis spectra were recorded on an UNISOKU RSP-601 stopped-flow spectrometer equipped with a MOS-type highly sensitive photodiode-array or on a Hewlett Packard 8453 diode array spectrophotometer equipped with a UNISOKU Scientific. Electrochemical measurements were performed on a CH Instrument (CHI630B) electrochemical analyser in deaerated CF_3CH_2OH/MeCN (1:1 v/v) containing 0.10 M Bu_4NPF_6 as a supporting electrolyte at 298 K. One-electron oxidation potentials of Ph_3P derivatives were determined by cyclic voltammetry (CV), differential pulse voltammetry (DPV) and second harmonic alternating current voltammetry (SHACV) techniques. A conventional three-electrode cell was used with a platinum working electrode (surface area of 0.3 cm^2) and a platinum wire as a counter electrode. The platinum working electrodes (BAS) were routinely polished with BAS polishing alumina suspension and rinsed with CF_3CH_2OH/MeCN (1:1 v/v) prior to use. The measured potentials were recorded as a function of $Ag/AgNO_3$ (0.01 M) reference electrode. All potentials (*versus* Ag/Ag^+) were converted to the values *versus* SCE by adding 0.29 V.[S5] All electrochemical measurements were performed under Ar atmosphere. X-band CW-EPR spectra were recorded at 5 K using an X-band Bruker EMX-plus spectrometer equipped with a dual mode cavity (ER 4116DM). Low temperatures were achieved and controlled with an Oxford Instruments ESR900 liquid

He quartz cryostat with an Oxford Instruments ITC503 temperature and gas flow controller. The experimental parameters for EPR spectra were as follows: Microwave frequency = 9.647 GHz, microwave power = 1.0 mW, modulation amplitude = 10 G, gain = 1×10^4, modulation frequency = 100 kHz, time constant = 40.96 ms, and conversion time = 85.00 ms. Product analysis for the oxidation of Ph_3P derivatives was performed on High Performance Liquid Chromatography (HPLC, DIOMEX Pump Series P580) equipped with a variable wavelength UV-200 detector.

Kinetic Measurements. Kinetic measurements for the oxygen atom transfer (OAT) reactions from **1** and **2** to a series of Ph_3P derivatives in CF_3CH_2OH/MeCN (1:1 v/v) at 273 K were performed on a UNISOKU RSP-601 stopped-flow spectrometer equipped with a MOS-type highly sensitive photodiode array or a Hewlett Packard 8453 photodiode-array spectrophotometer. The reactions were run in a 1-cm UV cuvette or a 1.0 cm optical path length of stopped-flow cell. The reactions of **1** (0.25 mM) and **2** (0.25 mM) with a series of Ph_3P derivatives were followed by monitoring absorption spectral changes of reaction solutions, and rate constants were determined by fitting the changes in absorbance at 800 nm for **1** and at 580 nm for **2**. In the oxidation of tri(*p*-tolyl)phosphine [(*p*-Me-Ph)$_3$P], tri(*m*-tolyl)phosphine [(*m*-Me-Ph)$_3$P], and Ph_3P by **1**, the second-order rate constants (k_{OAT}) were determined under second-order kinetic conditions due to fast reactions between **1** and Ph_3P derivatives. In the oxidation of tri(*o*-tolyl)phosphine [(*o*-Me-Ph)$_3$P] and tris(*p*-chlorophenyl)phosphine [(*p*-Cl-Ph)$_3$P] by **1**, the rates obeyed first-order kinetics under the pseudo-first-order reaction conditions ([substrate]/[**1**] > 10). In the case of **2**, all rates obeyed first-order kinetics under the pseudo-first-order reaction conditions ([substrate]/[**2**] > 10). Pseudo-first-order rate constants (k_{obs}) were linear for three or more half-lives with the correlation coefficient of $\rho > 0.99$. In each case, it was confirmed that the rate constants derived from at least three independent measurements agreed within an experimental error of ±10%. The pseudo-first-order rate constants, which were calculated by pseudo-first-order fitting of the kinetic data, increased proportionally with the concentrations of substrates, from which second-order rate constants (k_{OAT}) were determined. The kinetic experiments were run at least in triplicate, and the data reported represent the average values of these reactions.

Computational Details. Density functional theory (DFT) was applied at B3LYP/LACV3P*+//B3LYP/LACVP level[S6] using Gaussian 09.[S7] The high molecular charge (3+) made it necessary to perform the optimizations in solvent to avoid artificial results. The solvent (acetonitrile) effects were included using CPCM[S8] model with UFF cavity, per G09 default. As found for the $[(Bn\text{-}TPEN)Mn^{IV}(O)]^{2+}$ and redox-inactive metal ion-bound $[(Bn\text{-}TPEN)Mn^{IV}(O)]^{2+}$ complexes,[S9] the $[(Bn\text{-}TPEN)Mn^{IV}(OH)]^{3+}$ complex still has a quartet ground state (S = 3/2). Compared with the $[(Bn\text{-}TPEN)Mn^{IV}(O)]^{2+}$ complex, $[(Bn\text{-}TPEN)Mn^{IV}(OH)]^{3+}$ has a longer Mn-O bond and shorter Mn-N distances, which is similar to Sc^{3+} ion-bound $Mn^{IV}(O)$ complexes.[S9b] Benchmarks on the functional and the basis set have also been performed for the quartet ground state Mn^{IV}-OH species (Table S3). In all the cases, however, the final conclusion was consistent. In addition, the Mn-O distance is very short (1.75 Å) in the doublet excited state Mn^{IV}-OH species, but such species lies much higher than the quartet ground state by ca. 23 kcal/mol (Table S4). Thus, this excited state complex should not exist in the experimental conditions.

References

S1. W. L. F. Armarego and C. L. L. Chai, in *Purification of Laboratory Chemicals,* 6th ed., Pergamon Press, Oxford, 2009.

S2. H. Saltzman and J. G. Sharefkin, *Organic Syntheses*, Wiley, New York, 1973, Collect. Vol. V, pp. 658.

S3. (*a*) M. Lubben, A. Meetsma, E. C. Wilkinson, B. Feringa and L. Que Jr., *Angew. Chem. Int. Ed.*, 1995, **34**, 1512; (*b*) L. Duelund, R. Hazell, C. J. McKenzie, L. P. Nielsen and H. Toftlund, *J. Chem. Soc., Dalton Trans.*, 2001, 152; (*c*) S. Groni, P. Dorlet, G. Blain, S. Bourcier, R. Guillot and E. Anxolabéhère-Mallart, *Inorg. Chem*., 2008, **47**, 3166.

S4. X. Wu, M. S. Seo, K. M. Davis, Y.-M. Lee, J. Chen, K.-B. Cho, Y. N. Pushkar and W. Nam, *J. Am. Chem. Soc*., 2011, **133**, 20088.

S5. C. K. Mann and K. K. Barnes, *Electrochemical Reactions in Non-aqueous Systems*, Mercel Dekker, New York, 1970.

S6. (*a*) C. T. Lee, W. T. Yang and R. G. Parr, *Phys. Rev. B*, 1988, **37**, 785; (*b*) A. D. Becke, *J. Chem. Phys.*, 1992, **97**, 9173; (*c*) A. D. Becke, *J. Chem. Phys.*, 1992, **96**, 2155; (*d*) A. D.

Becke, *J. Chem. Phys.*, 1993, **98**, 5648; (*e*) The LACVP and LACV3P*+ basis sets uses pople style 6-31G and 6-311+G* basis sets (respectively) on all atoms except transition metals, where an ECP is used as defined in the quantum chemistry program Jaguar, version 7.7, Schrödinger, LLC, New York, NY, 2010; (*f*) P. J. Hay and W. R. Wadt, *J. Chem. Phys.*, 1985, **82**, 299; (*g*) K. G. Dyall, *Theor. Chem. Acc.*, 2004, **112**, 403.

S7. M. J. Frisch, G. W. Trucks, H. B. Schlegel, G. E. Scuseria, M. A. Robb, J. R. Cheeseman, G. Scalmani, V. Barone, B. Mennucci, G. A. Petersson, H. Nakatsuji, M. Caricato, X. Li, H. P. Hratchian, A. F. Izmaylov, J. Bloino, G. Zheng, J. L. Sonnenberg, M. Hada, M. Ehara, K. Toyota, R. Fukuda, J. Hasegawa, M. Ishida, T. Nakajima, Y. Honda, O. Kitao, H. Nakai, T. Vreven, J. A. Montgomery, Jr., J. E. Peralta, F. Ogliaro, M. Bearpark, J. J. Heyd, E. Brothers, K. N. Kudin, V. N. Staroverov, T. Keith, R. Kobayashi, J. Normand, K. Raghavachari, A. Rendell, J. C. Burant, S. S. Iyengar, J. Tomasi, M. Cossi, N. Rega, J. M. Millam, M. Klene, J. E. Knox, J. B. Cross, V. Bakken, C. Adamo, J. Jaramillo, R. Gomperts, R. E. Stratmann, O. Yazyev, A. J. Austin, R. Cammi, C. Pomelli, J. W. Ochterski, R. L. Martin, K. Morokuma, V. G. Zakrzewski, G. A. Voth, P. Salvador, J. J. Dannenberg, S. Dapprich, A. D. Daniels, O. Farkas, J. B. Foresman, J. V. Ortiz, J. Cioslowski and D. J. Fox, *R. D.01 Gaussian* 09, Gaussian, Inc., Wallingford, CT, 2013.

S8. (*a*) V. Barone and M. Cossi, *J. Phys. Chem. A.*, 1998, **102**, 1995; (*b*) M. Cossi, N. Rega, G. Scalmani and V. Barone, *J. Comput. Chem.*, 2003, **24**, 669.

S9. (*a*) X. Wu, M. S. Seo, K. M. Davis, Y.-M. Lee, J. Chen, K.-B. Cho, Y. N. Pushkar and W. Nam, *J. Am. Chem. Soc.*, 2011, **133**, 20088; (*b*) H. Yoon, Y.-M. Lee, X. Wu, K.-B. Cho, R. Sarangi, W. Nam and S. Fukuzumi, *J. Am. Chem. Soc.*, 2013, **135**, 9186.

Table S1 Comparison of the key geometric parameters for four ground state complexes

complex	Mn-O	Mn-N1	Mn-N2	Mn-N3	Mn-N4	Mn-N5
^{4}[(Bn-TPEN)Mn^{IV}(O)]^{a}	1.68	2.29	2.23	2.19	2.10	2.13
^{4}[(Bn-TPEN)Mn^{IV}(OH)]	1.79	2.09	2.06	2.00	2.01	2.09
^{4}[(Bn-TPEN)Mn^{IV}(O)]-(Sc^{3+})$_{1}$^{b}	1.75	2.10	2.08	2.01	2.02	2.11
^{4}[(Bn-TPEN)Mn^{IV}(O)]-(Sc^{3+})$_{2}$^{b}	1.75	2.09	2.08	2.01	2.02	2.10

^{a} Taken from reference 17b in the Text. ^{b} Taken from reference 17d in the Text.

Table S2 Mulliken spin density distribution

complex	Mn	O(H)	5×N	Rest of ligand	Sc_A	Sc_B	n×OTf
^{4}[(Bn-TPEN)Mn^{IV}(O)]^a	2.64	0.63	-0.15	0.02	-	-	-
^{4}[(Bn-TPEN)Mn^{IV}(OH)]	3.29	0.15	-0.56	0.12	-	-	-
^{4}[(Bn-TPEN)Mn^{IV}(O)]-$(Sc^{3+})_1$^{b}	3.13	0.27	-0.50	0.06	0.02	-	0.02^c
^{4}[(Bn-TPEN)Mn^{IV}(O)]-$(Sc^{3+})_2$^{b}	3.14	0.29	-0.54	0.08	0.01	0.00	0.03^d

^{a} Taken from reference 17b in the Text. ^{b} Taken from reference 17d in the Text. ^{c} n = 3. ^{d} n = 6.

Table S3 Benchmark on the functional and basis set for the quartet ground state Mn^{IV}-OH species

method	Mn-O	Mn-N1	Mn-N2	Mn-N3	Mn-N4	Mn-N5
B3LYP/LACVP	1.79	0.98	2.00	2.01	2.09	2.09
B3LYP/Def2-TZVP	1.78	0.97	2.01	2.03	2.10	2.11
B3LYP/Def2-TZVPP	1.78	0.97	2.02	2.03	2.10	2.11
BP86/Def2-SVP	1.78	0.98	2.00	2.02	2.11	2.10

Table S4 Key geometric parameters for the Mn^{IV}-OH species at different spin states computed at the B3LYP/LACVP level and the relative energies are calculated at the B3LYP/LACV3P+*//B3LYP/LACVP level

complex	Mn-O	Mn-N1	Mn-N2	Mn-N3	Mn-N4	Mn-N5	Δ***E***
^{2}[(Bn-TPEN)Mn^{IV}(OH)]	1.75	0.98	1.99	2.01	2.10	2.09	**22.8**
^{4}[(Bn-TPEN)Mn^{IV}(OH)]	1.79	0.98	2.00	2.01	2.09	2.09	**0.0**
^{6}[(Bn-TPEN)Mn^{IV}(OH)]	1.80	0.98	2.14	2.06	2.15	3.68	**5.9**

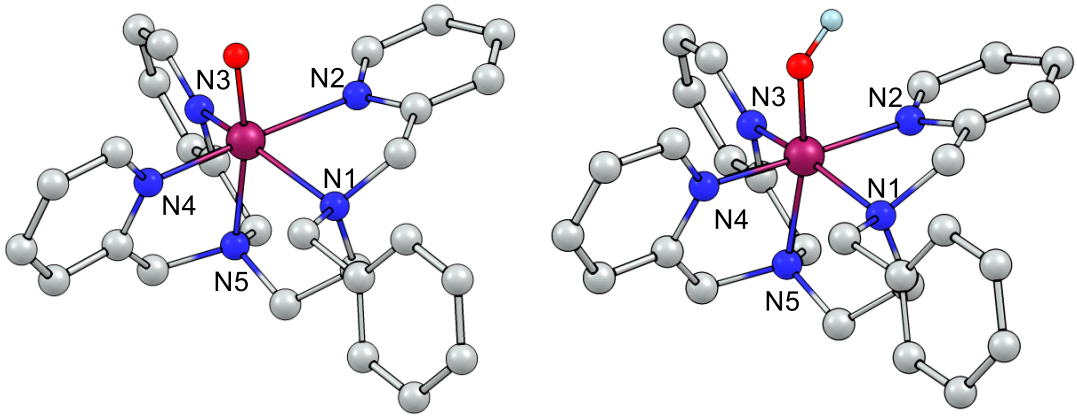

Fig. S1 DFT-optimized geometries for the $[(Bn\text{-}TPEN)Mn^{IV}(O)]^{2+}$ (left) and $[(Bn\text{-}TPEN)Mn^{IV}(OH)]^{3+}$ (right) species with S = 3/2 ground state obtained at the UB3LYP/LACVP level.

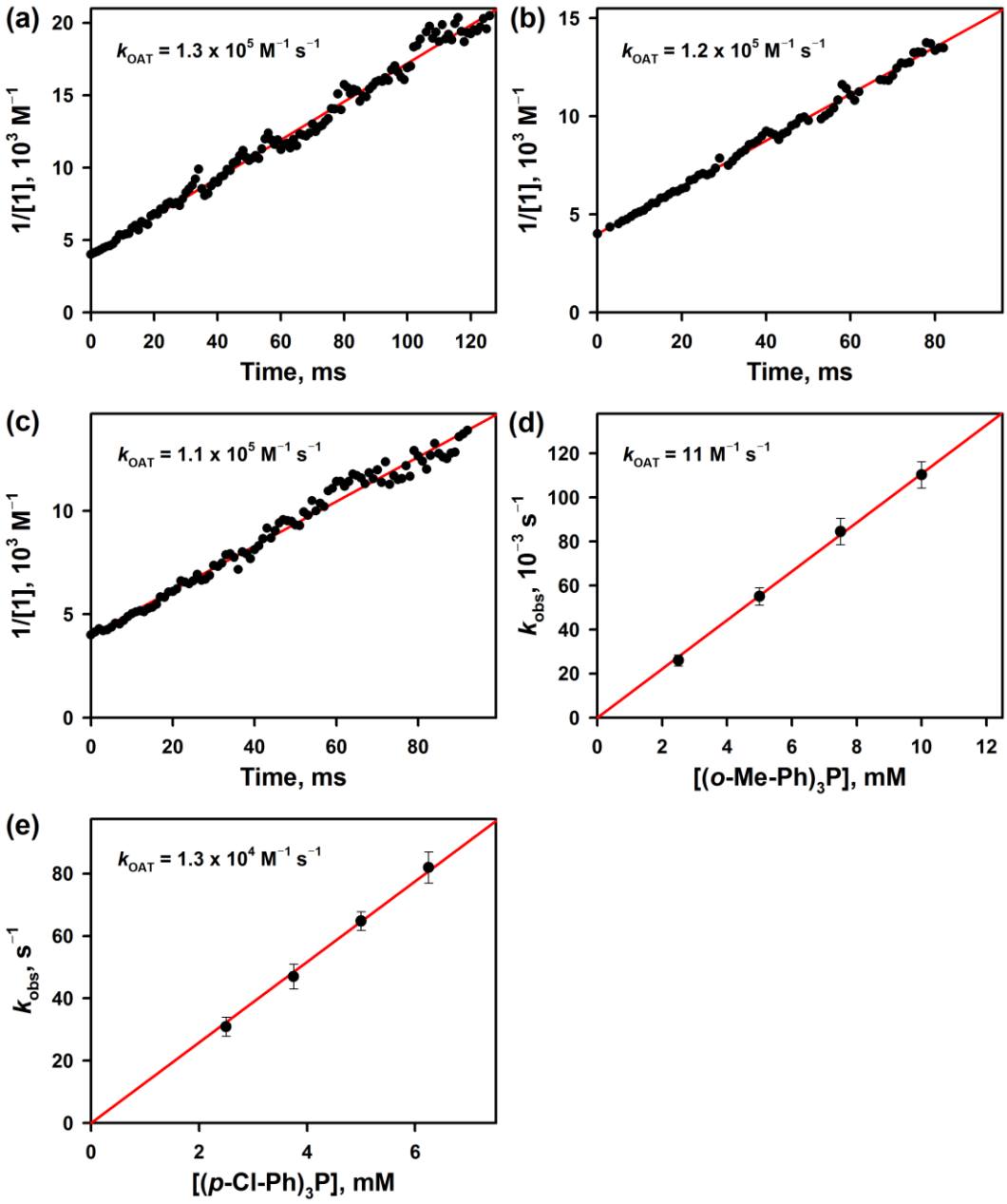

Fig. S2 (a, b, c) Second-order plot of 1/[**1**] *versus* time for OAT from **1** (0.25 mM) to Ph_3P derivatives [0.25 mM; (a) (*p*-Me-Ph)$_3$P, (b) (*m*-Me-Ph)$_3$P, and (c) Ph_3P] in CF_3CH_2OH/MeCN (1:1 v/v) at 273 K. (d, e) Plots of the pseudo-first-order rate constant (k_{obs}) against the substrate concentration to determine second-order rate constants (k_{OAT}) in the OAT from **1** (0.25 mM) to Ph_3P derivatives [(d) (*o*-Me-Ph)$_3$P and (e) (*p*-Cl-Ph)$_3$P] in CF_3CH_2OH/MeCN (1:1 v/v) at 273 K.

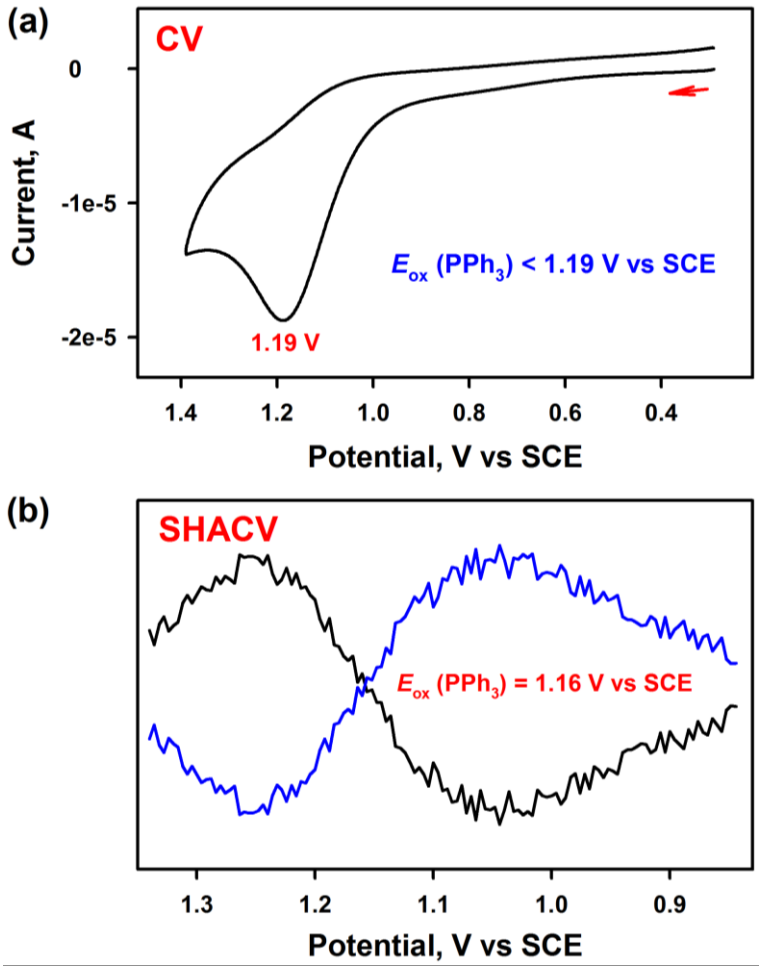

Fig. S3 (a) Cyclic voltammogram of Ph_3P (4.0 mM) with scan rate of 0.10 V/s in CF_3CH_2OH/MeCN (1:1 v/v) at 273 K. (b) Second-harmonic alternating current voltammogram (SHACV) of Ph_3P (4.0 mM) with scan rate of 4 mV/s in CF_3CH_2OH/MeCN (1:1 v/v) at 273 K.

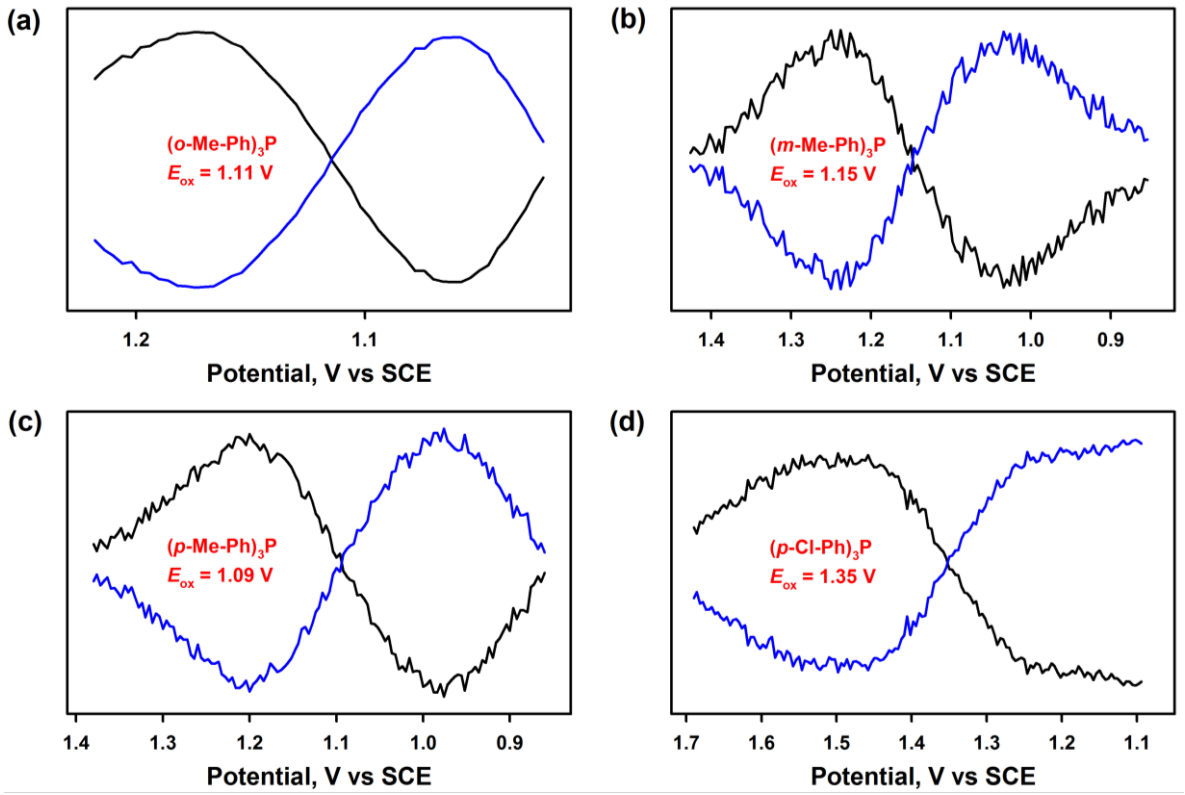

Fig. S4 Second-harmonic alternating current voltammograms (SHACVs) of (a) (*o*-Me-Ph)$_3$P (4.0 mM), (b) (*m*-Me-Ph)$_3$P (4.0 mM), (c) (*p*-Me-Ph)$_3$P (4.0 mM), and (d) (*p*-Cl-Ph)$_3$P (4.0 mM) with scan rate of 4 mV/s in CF_3CH_2OH/MeCN (1:1 v/v) at 273 K.

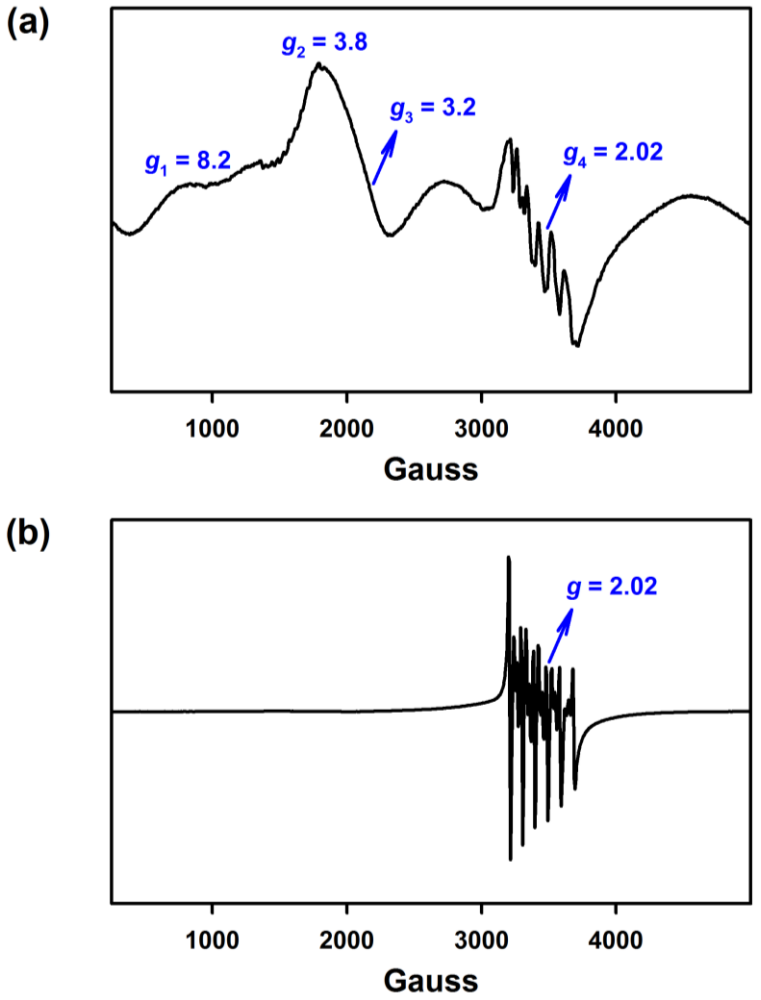

Fig. S5 X-band CW-EPR spectra of the complete reaction solutions obtained in the oxidation of Ph_3P (20 mM) by (a) **1** (1.0 mM) and (b) **2** (1.0 mM) in CF_3CH_2OH/CH_3CN (*v*/*v* = 1:1) at 273 K. Spectra were recorded at 5 K.

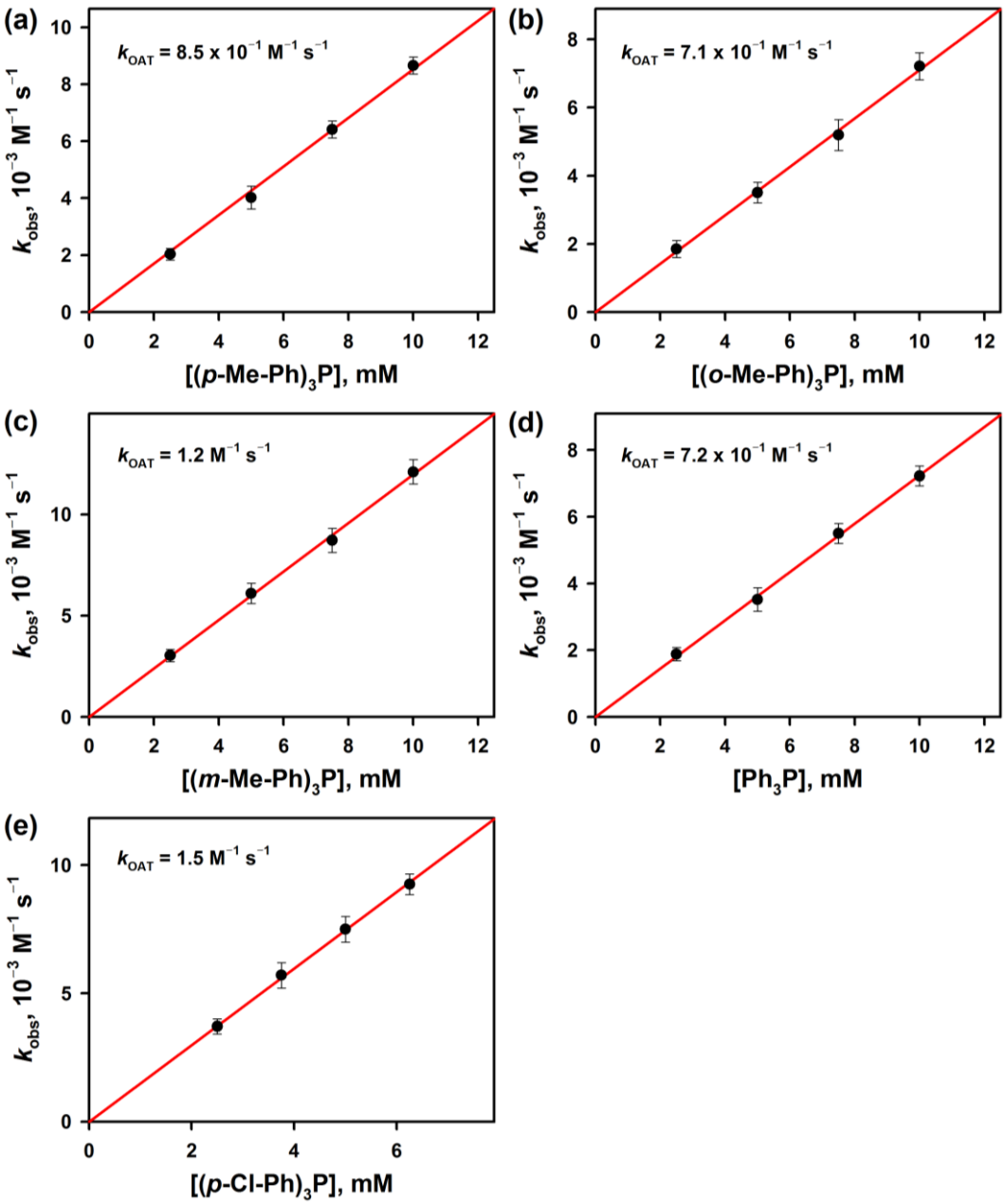

Fig. S6 Plots of the pseudo-first-order rate constant (k_{obs}) against the substrate concentration to determine second-order rate constants (k_{OAT}) in the OAT from **2** (0.25 mM) to Ph_3P derivatives [(a) (*p*-Me-Ph)$_3$P, (b) (*o*-Me-Ph)$_3$P, (c) (*m*-Me-Ph)$_3$P, (d) Ph_3P, and (e) (*p*-Cl-Ph)$_3$P] in CF_3CH_2OH/MeCN (1:1 v/v) at 273 K.

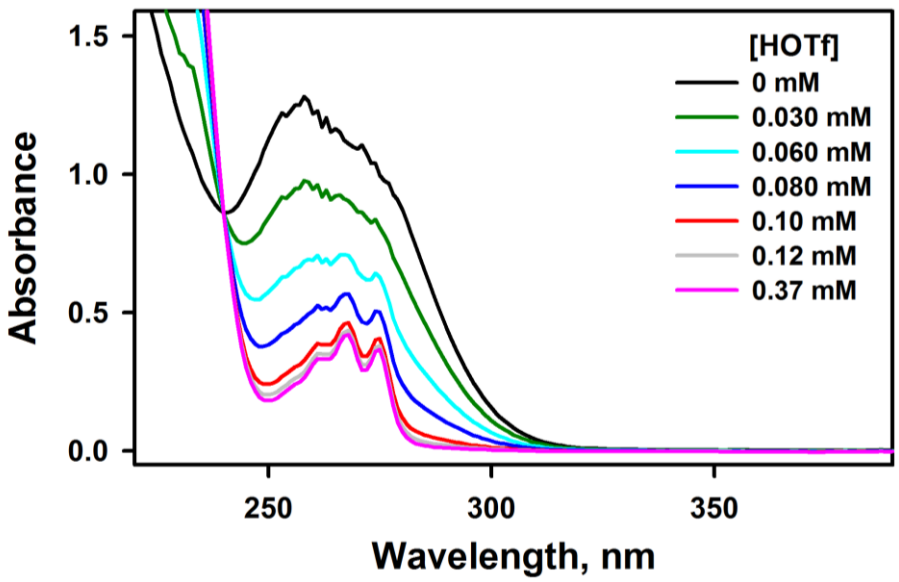

Fig. S7 UV-vis spectral changes observed in the titration of Ph_3P (0.10 mM; black line) with HOTf (0 – 0.37 mM) in CF_3CH_2OH/MeCN (1:1 v/v) at 273 K.

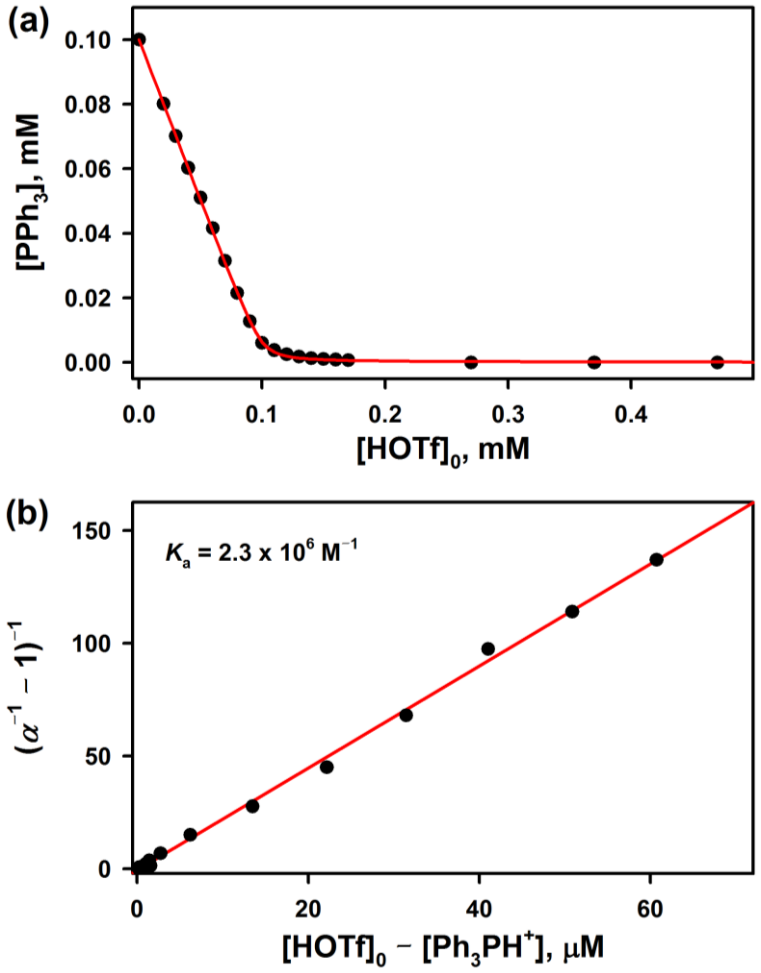

Fig. S8 (a) Plot of concentration of Ph_3P upon addition of HOTf (0 – 0.47 mM) to a solution of Ph_3P (0.10 mM) in CF_3CH_2OH/MeCN (1:1 v/v) at 273 K *versus* initial concentration of HOTf, $[HOTf]_0$. (b) Plot of $(\alpha^{-1} - 1)^{-1}$ *versus* $[HOTf]_0 - [Ph_3PH^+]$ ($\alpha = [Ph_3PH^+]/[Ph_3P]_0$) to determine the binding constant [$K_a = [Ph_3PH^+]/([Ph_3P]\times[HOTf])$] of HOTf to Ph_3P upon addition of HOTf (0 – 0.47 mM) to a CF_3CH_2OH/MeCN (1:1 v/v) solution of Ph_3P (0.10 mM) at 273 K.

The binding constant (K_a) is expressed by eqn (S1).

$$K_a = [Ph_3PH^+]/([Ph_3P]\times[HOTf]) \quad \text{(S1)}$$

Eqn (S2) is derived from eqn (S1), where $[HOTf]_0 = [HOTf] + [Ph_3PH^+]$, $[Ph_3P]_0 = [Ph_3P] + [Ph_3PH^+]$, and $\alpha = [Ph_3PH^+]/[Ph_3P]_0$. $[HOTf]_0$ and $[Ph_3P]_0$ are the initial concentrations of HOTf and Ph_3P, respectively.

$$(\alpha^{-1} - 1)^{-1} = K_a([HOTf]_0 - [Ph_3PH^+]) \quad \text{(S2)}$$

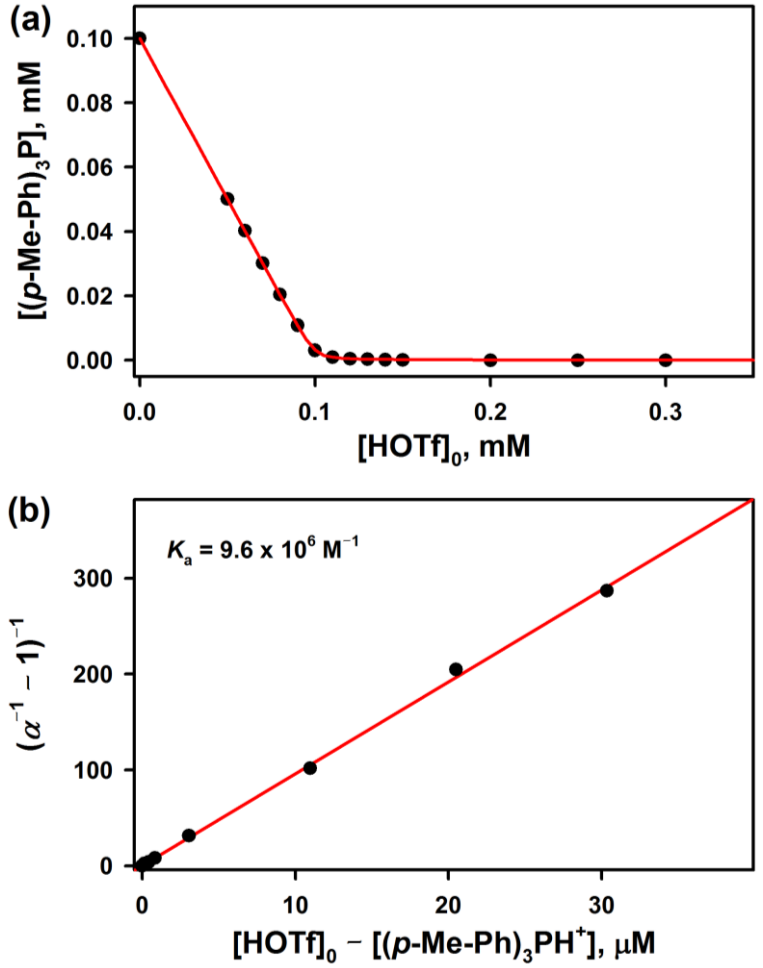

Fig. S9 (a) Plot of concentration of (p-Me-Ph)$_3$P upon addition of HOTf (0 – 0.30 mM) to a CF_3CH_2OH/MeCN (1:1 v/v) solution of (p-Me-Ph)$_3$P (0.10 mM) at 273 K *versus* initial concentration of HOTf, $[HOTf]_0$. (b) Plot of $(\alpha^{-1} - 1)^{-1}$ *versus* $[HOTf]_0 - [(p\text{-Me-Ph})_3PH^+]$ ($\alpha = [(p\text{-Me-Ph})_3PH^+]/[(p\text{-Me-Ph})_3P]_0$) to determine the binding constant [$K_a = [(p\text{-Me-Ph})_3PH^+]/([(p\text{-Me-Ph})_3P]\times[HOTf])$] of HOTf to ($p$-Me-Ph)$_3$P upon addition of HOTf (0 – 0.30 mM) to a CF_3CH_2OH/MeCN (1:1 v/v) solution of (p-Me-Ph)$_3$P (0.10 mM) at 273 K.

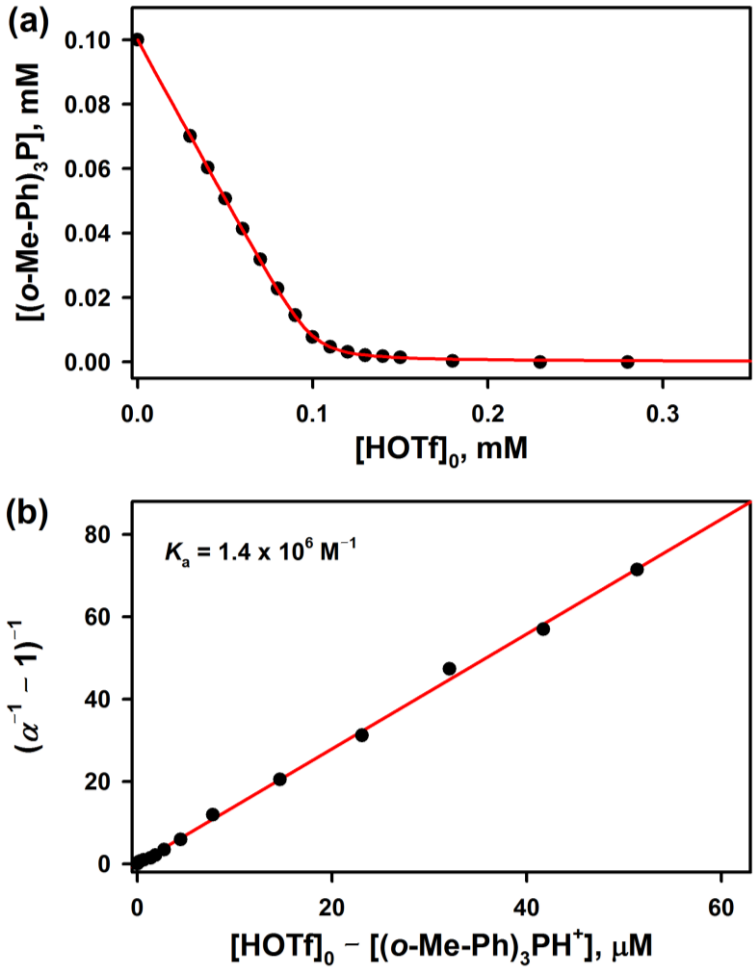

Fig. S10 (a) Plot of concentration of (*o*-Me-Ph)$_3$P upon addition of HOTf (0 – 0.28 mM) to a CF_3CH_2OH/MeCN (1:1 v/v) solution of (*o*-Me-Ph)$_3$P (0.10 mM) at 273 K *versus* initial concentration of HOTf, [HOTf]$_0$. (b) Plot of $(\alpha^{-1} - 1)^{-1}$ *versus* [HOTf]$_0$ – [(*o*-Me-Ph)$_3$PH$^+$] (α = [(*o*-Me-Ph)$_3$PH$^+$]/[(*o*-Me-Ph)$_3$P]$_0$) to determine the binding constant [K_a = [(*o*-Me-Ph)$_3$PH$^+$]/([(*o*-Me-Ph)$_3$P]×[HOTf])] of HOTf to (*o*-Me-Ph)$_3$P upon addition of HOTf (0 – 0.28 mM) to a CF_3CH_2OH/MeCN (1:1 v/v) solution of (*o*-Me-Ph)$_3$P (0.10 mM) at 273 K.

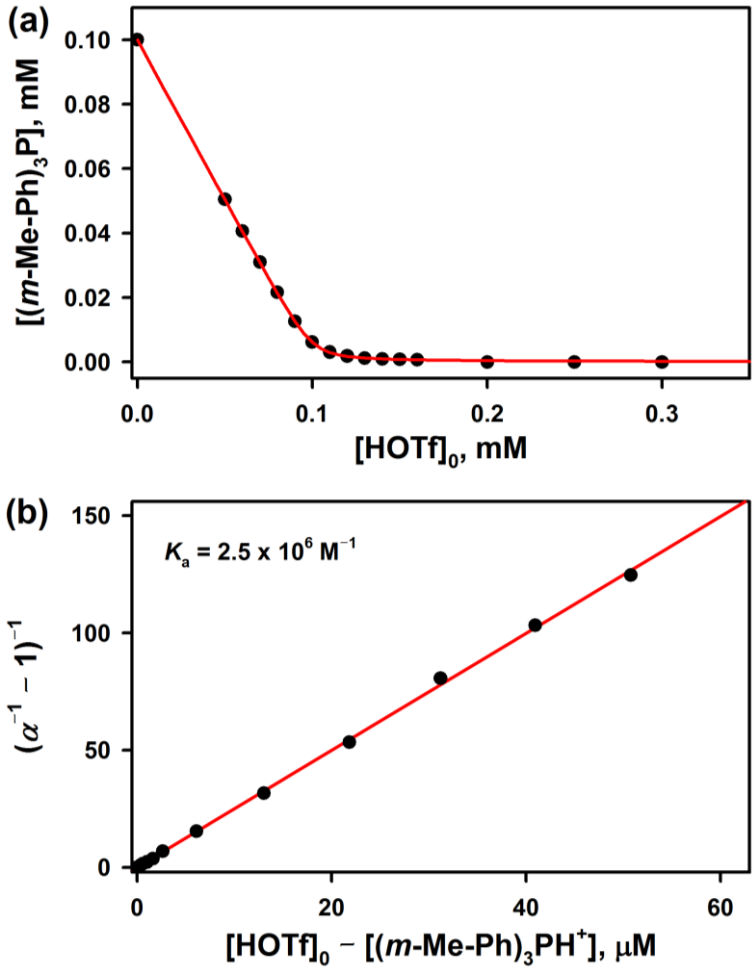

Fig. S11 (a) Plot of concentration of (*m*-Me-Ph)$_3$P upon addition of HOTf (0 – 0.30 mM) to a CF_3CH_2OH/MeCN (1:1 v/v) solution of (*m*-Me-Ph)$_3$P (0.10 mM) at 273 K *versus* initial concentration of HOTf, [HOTf]$_0$. (b) Plot of $(\alpha^{-1} - 1)^{-1}$ *versus* [HOTf]$_0$ – [(*m*-Me-Ph)$_3$PH$^+$] (α = [(*m*-Me-Ph)$_3$PH$^+$]/[(*m*-Me-Ph)$_3$P]$_0$) to determine the binding constant [K_a = [(*m*-Me-Ph)$_3$PH$^+$]/([(*m*-Me-Ph)$_3$P]×[HOTf])] of HOTf to (*m*-Me-Ph)$_3$P upon addition of HOTf (0 – 0.30 mM) to a CF_3CH_2OH/MeCN (1:1 v/v) solution of (*m*-Me-Ph)$_3$P (0.10 mM) at 273 K.

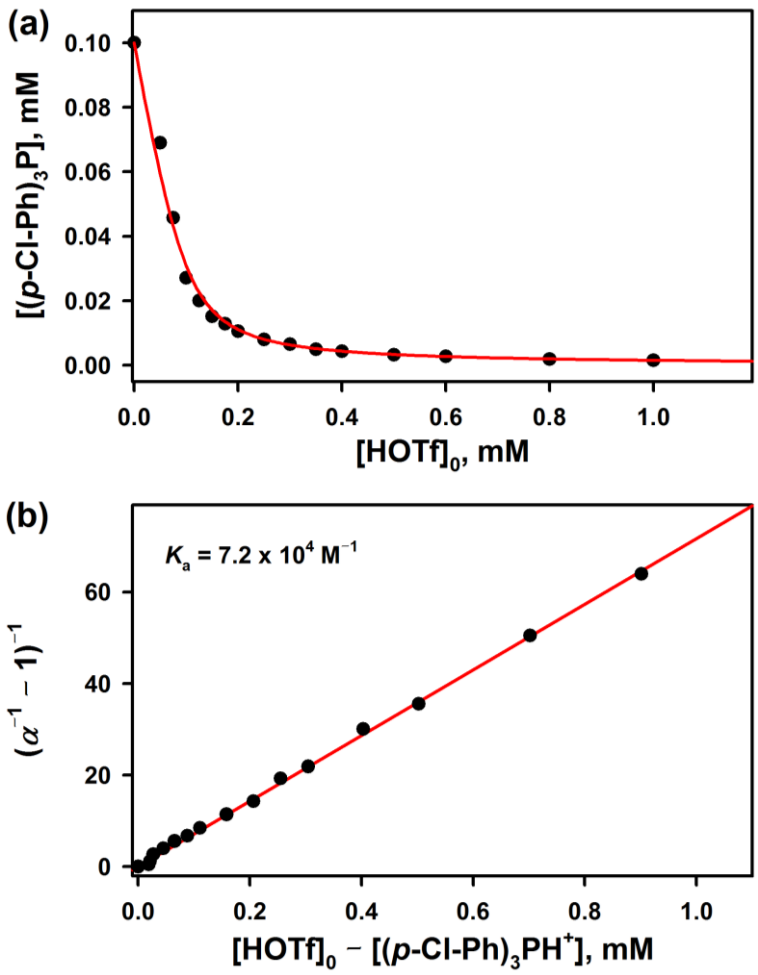

Fig. S12 (a) Plot of concentration of (p-Cl-Ph)$_3$P upon addition of HOTf (0 – 1.0 mM) to a CF_3CH_2OH/MeCN (1:1 v/v) solution of (p-Cl-Ph)$_3$P (0.10 mM) at 273 K *versus* initial concentration of HOTf, $[HOTf]_0$. (b) Plot of $(\alpha^{-1} - 1)^{-1}$ *versus* $[HOTf]_0 - [(p\text{-Cl-Ph})_3PH^+]$ ($\alpha = [(p\text{-Cl-Ph})_3PH^+]/[(p\text{-Cl-Ph})_3P]_0$) to determine the binding constant [$K_a = [(p\text{-Cl-Ph})_3PH^+]/([(p\text{-Cl-Ph})_3P]\times[HOTf])$] of HOTf to ($p$-Cl-Ph)$_3$P upon addition of HOTf (0 – 1.0 mM) to a CF_3CH_2OH/MeCN (1:1 v/v) solution of (p-Cl-Ph)$_3$P (0.10 mM) at 273 K.

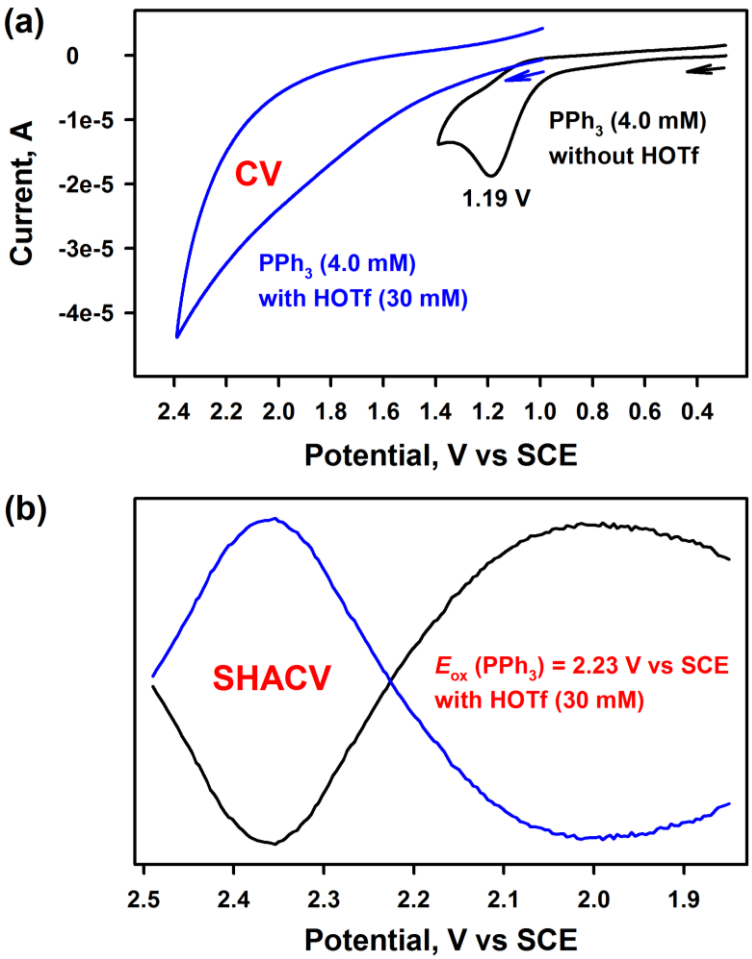

Fig. S13 (a) Cyclic voltammograms of Ph_3P (4.0 mM) with scan rate of 0.10 V/s in the absence (black line) and presence (blue line) of HOTf (30 mM) in CF_3CH_2OH/MeCN (1:1 v/v) at 273 K. (b) Second-harmonic alternating current voltammogram (SHACV) of Ph_3P (4.0 mM) with scan rate of 4 mV/s in the presence of HOTf (30 mM) in CF_3CH_2OH/MeCN (1:1 v/v) at 273 K.

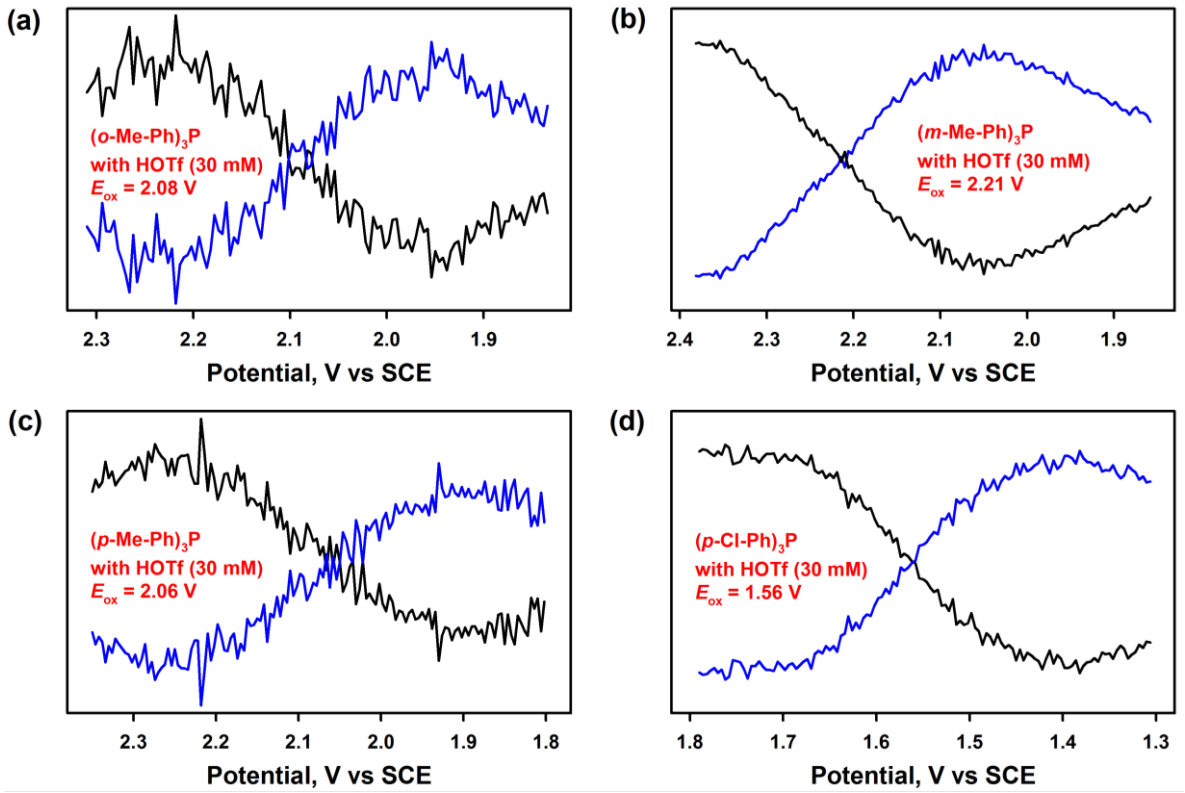

Fig. S14 Second-harmonic alternating current voltammograms (SHACVs) of (a) (*o*-Me-Ph)$_3$P (4.0 mM), (b) (*m*-Me-Ph)$_3$P (4.0 mM), (c) (*p*-Me-Ph)$_3$P (4.0 mM), and (d) (*p*-Cl-Ph)$_3$P (4.0 mM) with scan rate of 4 mV/s in the presence of HOTf (30 mM) in CF_3CH_2OH/MeCN (1:1 v/v) at 273 K.

Cartesian coordinates

^{2}I

25	7.535393000	10.179749000	3.397942000
7	8.330105000	11.955864000	2.969056000
7	6.544615000	10.870843000	5.007646000
7	5.942030000	11.157164000	2.434459000
7	6.386728000	8.472526000	3.053379000
7	8.579495000	9.341773000	1.838153000
6	9.370685000	12.496841000	3.655162000
1	9.736924000	11.944666000	4.508398000
6	9.926958000	13.707734000	3.250423000
1	10.755625000	14.123188000	3.807896000
6	9.403061000	14.362166000	2.129905000
1	9.824191000	15.303366000	1.799146000
6	8.316993000	13.802321000	1.442444000
1	7.879637000	14.302021000	0.587949000
6	7.790864000	12.592957000	1.881988000
6	6.603927000	11.885688000	1.284514000
1	5.900306000	12.583927000	0.822896000
1	6.899019000	11.156614000	0.525031000
6	5.322678000	12.174922000	3.379055000
1	4.270256000	12.315247000	3.120319000
1	5.818858000	13.138499000	3.235316000
6	5.509694000	11.733257000	4.795049000
6	4.747779000	12.213811000	5.857672000
1	3.921798000	12.886202000	5.664510000
6	5.072841000	11.823214000	7.160418000
1	4.491549000	12.187766000	7.998288000
6	6.156756000	10.961604000	7.368627000
1	6.441796000	10.646489000	8.363575000
6	6.876253000	10.496977000	6.273870000
1	7.722586000	9.832652000	6.369474000
6	4.888213000	10.148114000	2.009632000
1	4.409383000	10.480476000	1.083862000
1	4.124080000	10.135093000	2.787280000
6	5.520369000	8.785705000	1.839861000
1	4.760072000	8.008049000	1.728471000
1	6.156284000	8.750211000	0.955192000
6	7.395279000	7.407000000	2.688553000
1	6.882339000	6.542888000	2.260341000
1	7.891778000	7.085854000	3.608470000
6	8.387015000	7.990466000	1.730611000
6	9.098154000	7.227266000	0.809410000
1	8.911955000	6.163387000	0.738606000
6	10.042219000	7.851429000	-0.011792000
1	10.605514000	7.272985000	-0.733246000
6	10.244582000	9.229622000	0.109376000
1	10.965876000	9.750080000	-0.506224000
6	9.503213000	9.947962000	1.040839000
1	9.650318000	11.008266000	1.157011000
6	5.562723000	8.038331000	4.292884000
1	4.865911000	8.847472000	4.506140000
1	6.281061000	7.976082000	5.111087000
6	4.822249000	6.731029000	4.122330000
6	3.490129000	6.719412000	3.664585000
1	2.983751000	7.652305000	3.436192000
6	2.794406000	5.513264000	3.533912000
1	1.767758000	5.519508000	3.184724000
6	3.418610000	4.304072000	3.865578000
1	2.878566000	3.368768000	3.765663000
6	4.736509000	4.305839000	4.341327000
1	5.217139000	3.373962000	4.618192000
6	5.433364000	5.510752000	4.471452000
1	6.445904000	5.501313000	4.862931000
8	8.745668000	9.535736000	4.484078000
1	9.628589000	9.159215000	4.281765000

^{4}I

25	7.515266000	10.199165000	3.377561000
7	8.355799000	11.964119000	2.973037000
7	6.536190000	10.880389000	4.993502000
7	5.932926000	11.177868000	2.417923000
7	6.386377000	8.465832000	3.069372000
7	8.558497000	9.338337000	1.819061000
6	9.403673000	12.491378000	3.655528000
1	9.777003000	11.920713000	4.494011000
6	9.956263000	13.708804000	3.265583000
1	10.792112000	14.115414000	3.818666000
6	9.418296000	14.380674000	2.161918000
1	9.835154000	15.327654000	1.842251000
6	8.325102000	13.832360000	1.475033000
1	7.881695000	14.346384000	0.632178000
6	7.801126000	12.616947000	1.899387000
6	6.612175000	11.918255000	1.286162000
1	5.918072000	12.625597000	0.824237000
1	6.911054000	11.196468000	0.520820000
6	5.305353000	12.184423000	3.368659000
1	4.252415000	12.320915000	3.110122000
1	5.797057000	13.151693000	3.232119000
6	5.494234000	11.736369000	4.782684000
6	4.734591000	12.205735000	5.851199000
1	3.902724000	12.872840000	5.665273000
6	5.070720000	11.812615000	7.150873000
1	4.490410000	12.169763000	7.992618000
6	6.163717000	10.960777000	7.353156000
1	6.456093000	10.646624000	8.346183000
6	6.882949000	10.505107000	6.254450000
1	7.737472000	9.848310000	6.336473000
6	4.895311000	10.152492000	1.990467000
1	4.430484000	10.466921000	1.051439000
1	4.117776000	10.148271000	2.754861000
6	5.527490000	8.782682000	1.847275000
1	4.760821000	8.010444000	1.738967000
1	6.166073000	8.733817000	0.965458000
6	7.402500000	7.405622000	2.718157000
1	6.897881000	6.525891000	2.312216000

1	7.910839000	7.113046000	3.641218000
6	8.381729000	7.981671000	1.743796000
6	9.099794000	7.211578000	0.833774000
1	8.928462000	6.143965000	0.785880000
6	10.030160000	7.832130000	-0.005676000
1	10.598188000	7.246495000	-0.717512000
6	10.213152000	9.215341000	0.083996000
1	10.923229000	9.733148000	-0.546626000
6	9.467353000	9.943247000	1.004371000
1	9.600320000	11.007659000	1.098505000
6	5.556003000	8.032707000	4.298722000
1	4.853814000	8.839546000	4.505598000
1	6.267965000	7.974674000	5.123304000
6	4.817926000	6.722066000	4.129634000
6	3.488809000	6.705716000	3.665294000
1	2.979850000	7.636512000	3.433746000
6	2.797891000	5.496705000	3.529967000
1	1.773524000	5.499799000	3.173838000
6	3.423501000	4.289907000	3.865802000
1	2.886976000	3.352789000	3.763434000
6	4.737987000	4.296687000	4.349736000
1	5.220458000	3.366629000	4.629795000
6	5.429926000	5.504529000	4.484369000
1	6.439970000	5.498738000	4.882590000
8	8.737296000	9.515789000	4.488892000
1	9.620402000	9.183223000	4.226326000

^{6}I

25	8.064626000	10.796585000	3.783737000
7	8.680903000	12.478569000	2.621133000
7	7.018244000	11.287294000	5.485216000
7	6.208036000	11.417056000	2.891859000
7	5.726383000	8.027402000	3.141627000
7	8.580289000	9.245632000	2.368010000
6	9.836443000	13.161110000	2.818574000
1	10.485060000	12.781321000	3.597103000
6	10.150137000	14.278356000	2.047491000
1	11.078174000	14.808005000	2.218479000
6	9.247097000	14.697309000	1.062572000
1	9.466699000	15.565501000	0.452926000
6	8.049456000	13.995635000	0.874891000
1	7.329140000	14.310152000	0.130190000
6	7.792240000	12.881556000	1.672019000
6	6.551793000	12.033237000	1.549401000
1	5.704289000	12.622835000	1.184843000
1	6.718066000	11.220341000	0.835742000
6	5.728925000	12.510011000	3.849963000
1	4.687078000	12.761588000	3.633169000
1	6.329828000	13.404345000	3.662573000
6	5.920245000	12.065315000	5.272328000
6	5.103587000	12.451798000	6.332511000
1	4.230479000	13.065245000	6.149600000
6	5.436641000	12.036775000	7.628184000
1	4.814132000	12.326714000	8.465955000
6	6.574969000	11.248160000	7.832611000
1	6.857812000	10.917623000	8.823367000
6	7.353268000	10.886339000	6.735242000
1	8.251783000	10.292149000	6.823359000
6	5.058818000	10.429373000	2.750008000
1	4.304671000	10.900419000	2.110578000
1	4.616382000	10.305211000	3.739404000
6	5.375095000	9.041504000	2.134793000
1	4.458763000	8.692329000	1.649010000
1	6.152999000	9.087115000	1.375946000
6	7.094779000	7.501564000	3.335693000
1	7.021017000	6.409493000	3.326831000
1	7.391900000	7.775638000	4.360128000
6	8.116921000	7.955178000	2.328244000
6	8.610008000	7.042929000	1.394318000
1	8.221733000	6.032548000	1.379925000
6	9.601828000	7.435893000	0.488173000
1	9.989376000	6.731340000	-0.237071000
6	10.080423000	8.744420000	0.542528000
1	10.851816000	9.093727000	-0.130950000
6	9.550561000	9.618421000	1.490197000
1	9.904088000	10.635801000	1.560183000
6	4.657528000	7.470264000	4.015650000
1	3.796587000	8.136221000	3.959444000
1	5.036362000	7.465840000	5.041453000
6	4.303356000	6.058583000	3.558505000
6	3.434780000	5.867494000	2.468656000
1	3.005466000	6.719425000	1.950893000
6	3.099455000	4.572165000	2.060585000
1	2.423304000	4.430161000	1.224996000
6	3.635229000	3.464990000	2.730071000
1	3.377061000	2.461141000	2.410899000
6	4.500834000	3.652831000	3.817068000
1	4.902314000	2.797257000	4.348678000
6	4.839275000	4.945795000	4.229100000
1	5.492661000	5.085045000	5.084739000
8	9.617107000	10.606785000	4.667576000
1	10.090060000	9.751106000	4.710727000